

Journal of Materials Chemistry B

Accepted Manuscript



This is an *Accepted Manuscript*, which has been through the Royal Society of Chemistry peer review process and has been accepted for publication.

Accepted Manuscripts are published online shortly after acceptance, before technical editing, formatting and proof reading. Using this free service, authors can make their results available to the community, in citable form, before we publish the edited article. We will replace this *Accepted Manuscript* with the edited and formatted *Advance Article* as soon as it is available.

You can find more information about *Accepted Manuscripts* in the [Information for Authors](#).

Please note that technical editing may introduce minor changes to the text and/or graphics, which may alter content. The journal's standard [Terms & Conditions](#) and the [Ethical guidelines](#) still apply. In no event shall the Royal Society of Chemistry be held responsible for any errors or omissions in this *Accepted Manuscript* or any consequences arising from the use of any information it contains.

On the anti-tumor properties of biomedical magnesium metal

Yangmei Chen^{1,2}, Ming Xiao^{1,2}, Huan Zhao^{1,2}, Bangcheng Yang^{1,2*}

¹Engineering Research Center in Biomaterials, Sichuan University, Chengdu, 610064, China

²National Engineering Research Center for Biomaterials, Chengdu, 610064, China

yangbchengc@126.com

Abstract: H₂ is a therapeutic agent for tumors because it could scavenge free radical which is one of the accusations for this disease in human body. Biomedical magnesium (Mg) could release H₂ in the biodegradation process, so it might have antitumor properties. In this study, Mg metal (P-Mg) was subjected to anodic oxidation plus heat treatment to get AO-HT-Mg covered with MgO. In SBF experiments AO-HT-Mg showed bioactivity as it could induce calcium phosphate deposition. MgO layer played a protective role in the biodegradation process and controlled the H₂ releasing rate. In MRMT-1 rat breast carcinoma cell culture experiments, both P-Mg and AO-HT-Mg could inhibit free radical expression in the cells, and AO-HT-Mg showed higher inhibiting ability. In the animal experiments with 72 mice divided in 4 groups, both P-Mg and AO-HT-Mg could inhibit tumor growth. After implantation in the animals, P-Mg showed higher inhibiting ability at the initial stage, and the AO-HT-Mg showed higher inhibiting ability after 26 days. The tumor inhibiting properties depended on H₂ releasing rates. The results confirm Mg metal has antitumor properties *in vivo*, and it is

possible to optimize its antitumor properties by surface modification.

Key words: Magnesium; biodegradation; *in vivo* antitumor property; surface modification; carcinoma cell

1. Introduction

Magnesium (Mg) metal has been widely reported to be a potential biomaterial for tissue replacement and regeneration, especially for bony tissue and cardiovascular system, because of its biodegradation properties *in vivo*¹⁻³. After Mg metal is implanted in the body, it will be absorbed and replaced by the regenerative tissues. During the biodegradation, by-products including Mg^{2+} and H_2 will be produced and give a heavy influence on the tissue response *in situ*⁴⁻⁶. It has been reported that H_2 would induce fracture of bone in the bony tissue and destroy of vascular stents in the cardiovascular system^{7,8}. So the topics about biomedical Mg research in the past decades mainly focused on its biodegradation so as to achieve the prevention from the negative effects of H_2 .

In recent years, it has been reported that H_2 is a therapeutic agent for free radical relating diseases, including cancers, senile diseases and so on⁹⁻¹². H_2 could scavenge the free radicals, especially the reactive hydroxyl radicals (OH) and peroxynitrite ($ONOO^-$), which are accusations for these diseases¹³. In a research of Ohsawa and his colleagues, they reported that H_2 scavenged the reactive hydroxyl radicals according to the

following reaction (1)¹⁴:



After the free radicals were scavenged, the diseases concerning with them were significantly restrained.

As the biomedical Mg could release H₂ during the biodegradation, it is logical to assume that Mg metal is a potential material with therapeutic properties to inhibit the free radical relating diseases. So in our previous study, we proposed that Mg might be a potential biomaterial with anti-tumor properties, and we found H₂ released from Mg was effective to scavenge free radical in the Fenton reaction system and osteosarcoma cells¹⁵.

In order to confirm the anti-tumor properties of Mg metal in detail, we studied the anti-tumor properties of biomedical Mg *in vivo* in this study. Anodic oxidation plus heat treatment surface modification method was employed to control the biodegradation of Mg.

2. Experimental section

2.1 Surface modification and characterization of Mg metal

Commercial pure Mg metal (P-Mg, 99.95%) was used for this study. Mg plates (10mm×10mm×1mm) were polished with 400 grit, 800 grit, and 1000 grit sandpaper, then ultrasonically cleaned with acetone, ethanol, and distilled water three times individually in turn. The as-received plates were subjected to anodic oxidation plus heat treatment as the reference

described¹⁶. The anodic oxidation treatment was performed at a galvanostatic model of 0.05 A in 1 L KOH solution (1M in concentration) for 30 min at room temperature. The samples were further heat treated at 500°C for 1h so as to change the Mg(OH)₂ to MgO on the surface. We defined the as-received metal after this modification as AO-HT-Mg. Both P-Mg and AO-HT-Mg were analyzed with X-ray diffraction (XRD, DX-1000 X-ray diffract meter) and scanning electron microscopy (SEM, HITACHI-S4800, JAPAN) to characterize the surface changes of Mg metals after the treatments. XRD analysis was carried out with Cu K α radiation working with 40 kV and 25 mA. The 2θ range varies from 20° to 80° at a scanning rate of 0.02°/s. SEM observation was performed with an accelerating voltage of 30 kV.

2.2 Biodegradation of Mg metals *in vitro*

In order to study the bioactivity of P-Mg and AO-HT-Mg, they were soaked in 10 mL simulate body fluid (SBF) at 37 °C for 24h, then they were analyzed with XRD and SEM. SBF was prepared by dissolving NaCl, NaHCO₃, KCl, K₂HPO₄·3H₂O, MgCl₂·6H₂O, CaCl₂·2H₂O, and Na₂SO₄ in distilled water, and adjusting the pH value to 7.4 with 1M HCl and Tris, according to the method of Kokubo¹⁷. In order to investigate the biodegradation of both metals, the metals were soaked in 50mL SBF for 85 h, according to the requirement of ASTM G31-72. The pH values of the solutions and the amounts of H₂ released from the degradation

were monitored every 3h. The pH value was detected by a pH meter (Mettler Toledo, FE20, Swiss). For each time point, at least 3 samples were studied to get average data.

2.3 *In vitro* anti-tumor properties of Mg metals

2.3.1 Breast carcinoma cell culture

In order to study the anti-tumor properties of Mg *in vitro*, MRMT-1 rat breast carcinoma cells at the 7th passage were employed to study the effects of Mg on the free radicals expression in the cells. MRMT-1 cells were cultured in Dulbecco's modified Eagle's medium (DMEM, Gibco, USA) containing 10% new born calf serum and 1% antibiotic under 5% CO₂ atmosphere at 37°C. After P-Mg and AO-HT-Mg were subjected to radiation sterilization for 21h at 25K Gy (FJX424, Co₆₀ γ rays), specimens were put in 12-well plates, and 3mL medium were put into each well to balance the surface for 24h, according to our previous study¹⁵. During the balance procedure, the medium was replaced with fresh medium every 4h. The purpose of balance the surface was to make the surface suitable for cells survival. After the balanced metals were dried with cold air, they were put in 24-well plates again, and 2 mL cell suspension (1.5×10^5 cells/mL) were added onto the metal plates to culture for 1, 2 and 3 d. A group of wells without any material was also cultured with cells, which were set as control. The medium was replaced every 24h during the culture. At 1, 2 and 3 d, the cell-cultured samples

were taken out from the culture plate and washed with PBS two times. Then the cells were stained with 5 μ g/mL fluorescein diacetate for CLSM (Leica.SP5, Germany) analysis to investigate their attachment and growth on the metals.

2.3.2 Detection of free radicals in cell

ROS Assay Kit (Beyotime, CHINA) was used to detect the levels of free radicals in MRMT-1 cultured on metal surfaces and blank wells. At 1, 2 and 3 d, the culture medium in 24-well plates was removed, and 300 μ L 0.25% trypsin/ 1 mM EDTA solution was added into each well and swirled to cover the entire sample, then 1 ml serum-free medium was added to harvest the cells from plate. The cells were transferred to conical tube and centrifuged for 5 min (1200 rpm) at room temperature to collect the cells. After the supernatant was discarded, dichlorofluorescein diacetate (DCFH-DA) diluted to 1000 times with serum-free medium was put into the conical tube for 30 min incubation in oscillator at 37 $^{\circ}$ C. DCFH-DA is an uncharged, cell permeable fluorescent probe. Inside the cells DCFH-DA is cleaved by nonspecific esterases to form DCFH, which is oxidized to the fluorescent compound 2', 7'-dichlorofluorescein (DCF) in the presence of ROS. The DCFH-DA supernatant was removed from the conical tube by centrifuging, and the cells were washed with serum-free medium three times to remove the residual DCFH-DA. Finally, the average content of free radicals in single cell was measured at 488 nm

(excitation wavelength) and 525 nm (emission wavelength) by flow cytometry assay (FCA, BECKMAN, Cytomic Fc500, America).

2.4 *In vivo* anti-tumor properties of Mg metal

2.4.1 Animal experiment

In order to investigate the anti-tumor properties of Mg metals *in vivo*, 100 μ L 4T1/Luc cells (1×10^7 cells/mL) was subcutaneously injected in 8-week-old female BALB/c mouse (about 20g in weight, Sichuan University) to prepare transplantable tumor *in situ*. During the animal experiments, the animals were divided into 4 groups randomly with 18 mice in each group. Three groups of mice were anaesthetized with an intraperitoneal injection of 1% sodium pentobarbital. The back skins were shaved and disinfected with 75% ethanol. Two groups among them were exposed the back muscles after the skin incision. P-Mg and AO-HT-Mg were subcutaneously implanted in the animals and fixed on the muscles by sutures respectively. After the wounds were closed, both groups of mice were subcutaneously injected with 4T1/Luc cells just near the metals. In the meantime, another anaesthetized group mice without implant were also subcutaneously injected with 4T1/Luc cells as control group. The group without any surgery was used as blank group.

These experiments were conducted in accordance with the Guidelines for Animal Experimentation (National Engineering Research Center for Biomaterial, Sichuan University), regarding the care and use of animals

in the experimental procedures, and the experiments have been approved by the institutional committee of National Engineering Research Center for Biomaterial, Sichuan University.

2.4.2 General observation

After operation, the wound cicatrisation state of animals was observed. After 7d, tumor volume was measured every 3 or 4 d. The sizes of tumors were monitored with the following method (2), which had been widely used in references¹⁸⁻²⁰.

$$S = W^2 \times L/2 \quad (2)$$

S, W and L are the size, width, and length of tumor respectively. The tumor growth rate was calculated with the sizes of the tumors.

2.4.3 *In vivo* imaging analysis

At 10, 20 and 30d after the operation, the animals with tumors were intraperitoneally injected with 10 μ L/g D-Luciferin potassium salt (15mg/mL in DPBS, Fanbo Biochemical, China). Ten min later, the animals were anaesthetized with sodium pentobarbital for the analysis with an *in vivo* imaging system (Maestro Ex Pro System, USA).

2.4.4 Malondialdehyde evaluation

At 10, 20 and 30d after the operation, 6 animals of each group were sacrificed at every time points. The blood of the animals were collected,

and the malondialdehyde (MDA) in serum was analyzed with mouse MDA ELISA Kit (R&D, USA). The operation of analysis procedure for MDA was according to the instruction of the Kit. MDA level is a characteristic factor for ROS in serum. Higher ROS would result in higher MDA level in serum²¹.

2.4.5 Histological evaluation

After the animals were sacrificed, the tumors induced by 4T1/Luc cells were collected. The weights of the tumors were analyzed with an electronic balance. And the tumors were fixed with 4% paraformaldehyde with pH value 7.4 for 24 h and dehydrated in gradient alcohols (70, 80, 90, 95, and 100 %), and then embedded in paraffin. After it was cut into sections with thickness of 3 μm , it was stained with hematoxylin and eosin (HE), and observed under an optical microscope.

2.5 Statistical analysis

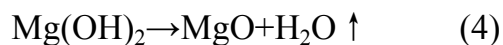
The results were statistically studied with SPSS11.0 software and the corresponding *p*-values were considered to be significant at values less than 0.05. All the statistical analysis was performed with at least three samples for each single experiment.

3 Results

3.1 Mg metal surface characterization

XRD and SEM were used to characterize the surface structures of P-Mg

and AO-HT-Mg. The SEM photographs (Figure 1(A, B)) showed the P-Mg had a smooth surface, and the anodic oxidation plus heat treatment made the metal surface porous. From the XRD spectra (Figure 1(C)), it was clear that only peaks of Mg could be found in P-Mg. For AO-HT-Mg, peaks of MgO appeared, besides the peaks of Mg. It indicated that the AO-HT-Mg was covered with a layer of MgO. In previous study, it had been proved that Mg(OH)₂ would be formed on the surface by the anodic oxidation treatment (3)²². MgO on the metal surface was formed by the decomposition of Mg(OH)₂ during the heat treatment (4).



The escaping of water vapor during the heat treatment would cause the porous structure of MgO.

3.2 Biodegradation of Mg metal

In order to examine the mineralization ability of modified samples, P-Mg and AO-HT-Mg were soaked in SBF for 24 h and presented by the SEM photographs and XRD spectra (Figure 2). It was clear that AO-HT-Mg was covered by a layer of mineral (Figure 2(A, B)). Some cracks appeared in the mineral. It indicated that mineral deposition happened on its surface during the biodegradation procedure in SBF. Only some corrosion pits could be found on P-Mg. The XRD spectra (Figure 2(C)) showed that peaks of both Mg and Ca₂P₂O₇ appeared on the surface of

AO-HT-Mg, and the peaks of MgO disappeared from the spectra of AO-HT-Mg after it was soaked in SBF for 24 h. Only peaks of Mg and Mg(OH)₂ could be found in the spectrum of P-Mg after it was soaked in SBF for 24h. It also showed the crystallinity of P-Mg surface decreased after the SBF soaking. It indicated that reaction between P-Mg and water happened. The calcium phosphate formation on the AO-HT-Mg indicated its bioactivity in biological environment. Ca₂P₂O₇ is the intermediate phase for apatite that is essential for a bioactive bonding between the biomaterials and bone. The porous surface structure of AO-HT-Mg could provide much more nucleation site, which might be beneficial for calcium phosphate formation in SBF.

Immersion corrosion testing of Mg metals showed that the AO-HT-Mg presented the stronger ability to resist corrosion (Figure 3). For the SBF soaked with P-Mg (Figure 3(A)), the pH value increased steadily from 7.4 to 8.2 in the initial 30h, after that it increased sharply to 9.8 in 15 h, and then the pH value became stable. For the SBF soaked with AO-HT-Mg (Figure 3(A)), the pH value increased steadily from 7.4 to 8.5 after it was soaked with AO-HT-Mg for 85h. The pH value of the SBF soaked with P-Mg was higher than that of AO-HT-Mg. It is well known that Mg(OH)₂ which is the products of Mg degradation would increase the pH value of SBF. This result indicated the degradation of AO-HT-Mg was slower than P-Mg. The anodic oxidation plus heat treatment was an

effective method to control the biodegradation of Mg metal. It is obvious that the H₂ releasing rate of AO-HT-Mg was much slower than that of the P-Mg (Figure 3(B)). It is logically to realize H₂ control releasing by controlling the biodegradation of Mg through the surface modification.

MgO formed on Mg metal by anodic oxidation plus heat treatment provided a protective role for the metal degradation. Additionally, calcium phosphate formed on the surface in SBF might also provide a protective role for the metal.

3.3 *In vitro* anti-tumor properties of Mg metals

In the studies of our laboratory, we have confirmed the cells could not survive on the Mg metal if it had not been subjected to balancing in cell culture medium, where the high pH in the medium resulted from the biodegradation made the environment not suitable for cell survival¹⁵. After the balancing procedure in medium for 24h, a biomimetic coating formed on both surfaces (Figure 4) and the pH value of medium decreased to 8.2. It is reported the biomimetic coating formed in medium could protect Mg metal²³. It is obvious that the protective role of the biomimetic coating could not change the biodegradation trends for both Mg metals, although it is an effective method to make the surfaces of both Mg metals suitable for cell survival.

The MTT results showed the proliferation of MRMT-1 cells on P-Mg, AO-HT-Mg and control plates (Figure 5). From the figure, it was clear

that the OD values of cells on both P-Mg and AO-HT-Mg were significantly lower than that of the control all the time ($p < 0.05$). It was the by-products of $\text{Mg}(\text{OH})_2$ that inhibited the cell growth and proliferation. At 1 d and 3 d, the OD values of MRMT-1 cells on AO-HT-Mg were significantly higher than that on P-Mg ($p < 0.05$). It indicated that the cells on AO-HT-Mg proliferated faster than that on P-Mg metal, although the OD values of the cells on P-Mg and AO-HT-Mg had no statistically significant difference at 2d.

The MRMT-1 cells adhesion on P-Mg, AO-HT-Mg and control plates were presented in figure 6. At 1 and 2d, the cells on the surfaces of P-Mg and AO-HT-Mg exhibited sphere-like characteristic. At 3d, the cells on the surfaces of P-Mg and AO-HT-Mg exhibited spreading better with characteristic spindle-like morphology. Compared to cells cultured for 1 and 2 d, the cells on the surfaces of P-Mg and AO-HT-Mg exhibited larger spreading at 3d, and the cells on the surfaces of AO-HT-Mg exhibited spreading better than that on P-Mg. The results showed that cells cultured on the surface of AO-HT-Mg had better proliferation and extending than that on P-Mg.

Both MTT and CLSM results indicated that P-Mg and AO-HT-Mg could support cell growth and proliferation. The AO-HT-Mg was more suitable for cell growth and proliferation than P-Mg. This result indicated the protective role of MgO layer on AO-HT-Mg is also beneficial for the cell

growth on the metal surfaces, which might improve the biocompatibility of biomedical Mg metal in clinical application.

After the MRMT-1 cells were cultured for 1, 2 and 3d, the average OD values of free radicals in single cell on P-Mg and AO-HT-Mg groups were significantly lower than the control group ($p < 0.05$) (Figure 7). At 1 d, the average OD value of cells on P-Mg was higher than that on AO-HT-Mg, but there was not statistical significant difference between them. At 2 and 3d, the average OD values of cells on P-Mg was significantly higher than that on AO-HT-Mg ($p < 0.05$). It was also obvious that the OD values increased with time. This results indicated that the free radicals in single cell on P-Mg and AO-HT-Mg was less than that of control, and the free radicals in single cell on AO-HT-Mg was less than that on P-Mg. The free radicals in the cells had an order of AO-HT-Mg < P-Mg < control.

3.4 *In vivo* anti-tumor properties of Mg metals

After the 4T1/Luc cells were subcutaneously injected in the animals for 7 d, it could be found that transplantable tumor was successfully prepared on the backs of animals (Figure 8). For all the groups of animals injected with 4T1/Luc cells, the tumors grew with time and it became cankerous at 13 d. The canker became more serious with time for all the tumors.

It was obvious that the tumor sizes of the animals implanted with P-Mg or AO-HT-Mg were smaller than that of control, except at the initial stage

(Table1). With the size of the tumors, we calculated the tumor growth rate according to the following method (5):

$$V_g = (\Delta S/S)/\Delta t \quad (5)$$

Where V_g is the tumor growth rate, S is the tumor size at t day, ΔS is the tumor size change during Δt d, $\Delta t=3$ or 4 d.

For all the time, the tumor growth rate of the control group is significantly larger than both groups implanted with P-Mg or AO-HT-Mg ($p<0.05$) (Figure 9). In this figure, it was also interesting that the tumor growth rate of the animals implanted with P-Mg was slower than the AO-HT-Mg group till 26 d. After that time, the tumor growth rate of P-Mg group was significantly faster than the AO-HT-Mg group. In the *in vivo* imaging analysis, it could also be found both P-Mg and AO-HT-Mg could inhibit the tumor growth (Figure 10). The trend of weight change kept consistent with the growth of tumor sizes in different groups of animals (Figure 11). The MDA level in the serums reflected the concentration of free radicals of different groups of animals at 10, 20 and 30 d *in vivo*. For all the time, the control group injected with 4T1/Luc cells without Mg implant had the significant highest MDA level (Figure 12). The blank group was normal animals which were not treated with 4T1/Luc cells or Mg metal. In figure 12, we could find the animal groups implanted with P-Mg and AO-HT-Mg had a significant lower MDA level than the blank group, and the P-Mg group had a significant lower MDA

level trend than the AO-HT-Mg group. The MDA levels in different groups of animals had an order of P-Mg<AO-HT-Mg<Blank<Control. It indicated both P-Mg and AO-HT-Mg had the ability to inhibit the MDA level in animals, and P-Mg had a higher ability than the AO-HT-Mg.

To evaluate whether tumor growth inhibition by the Mg metals was related to apoptosis, HE staining (Figure 13) was carried out. At 10 d post-operation, for the control group injected with 4T1/Luc cells, most of the cells were stained with blue color, which indicated they were live (Figure 13(A1)). In the groups implanted with P-Mg and AO-HT-Mg, some cells were stained with red color at this time, which indicated they were dead (Figure 13(B1, C1)). It also presented a certain range of cell death areas surrounding the tumor for the control group at 20 and 30 d post-operation (Figure 13(A2, A3)). In the groups implanted with P-Mg and AO-HT-Mg, the cell death areas increased along with time and large zones of cell death were presented surrounding the tumor at 30 days (Figure 13(B2, C2, B3, C3)). The cell death area was calculated by Image-Pro Plus analysis software (Figure 14). Both P-Mg and AO-HT-Mg groups showed significant higher cell death rates than control group ($p < 0.05$), and P-Mg group showed significant higher cell death rate than AO-HT-Mg group ($p < 0.05$). The results indicated both P-Mg and AO-HT-Mg could promote cell apoptosis and necrosis within tumor and reduce the rate of tumor progression, and P-Mg had higher ability than

AO-HT-Mg.

4 Discussion

In the past decades, it has been found that the free radicals in the body are important factor for tumor transplantation and recurrence²⁴⁻²⁶. Some researchers have reported the agents with the abilities to scavenge free radicals had the potential to treat tumors²⁷. For example, gallic acid and hesperidin complex^{28,29}, which are all clinically used medicines for tumor treatment, have been proved to have the ability to scavenge free radicals in the body.

Since 1970's, it has been found that H₂ had the ability to scavenge free radicals in the body¹¹. So many reports showed it is an effective agent to treat diseases concerning with free radicals. For example, Dole et al reported that H₂ could cause the regression of skin tumor in hairless albino mice, because it is a free radical decay catalyzer¹¹. Saitoh et al reported H₂ could inhibit tumor cell growth because it could scavenge intracellular oxidants³⁰.

Mg could release H₂ during the biodegradation. In this study, the biodegradation of Mg in biological environment was successfully regulated by surface modification, which caused a controllable H₂ releasing process. The MgO layer formed on the Mg surface by anodic oxidation plus heat treatment plays a protective role for Mg degradation. The results also indicated the MgO prepared in this study could induce

bioactive response as samples treated by alkali- heat treatment we reported in our previous study¹⁵.

In this study, it is very interesting that AO-HT-Mg showed higher ability than P-Mg to scavenge free radical in cells, although it has slower H₂ releasing rate. It might relate with the high pH environment around the materials. It was reported that high pH environment could cause cell apoptosis and necrosis due to free radicals accumulation in cells^{31,32}. High pH environment around P-Mg would induce more free radicals in cells, which made the single cell accumulate more free radicals. The balance of pH value and H₂ made the AO-HT-Mg had better ability of scavenging free radicals in cell culture experiments.

For the *in vivo* test, both P-Mg and AO-HT-Mg showed the abilities to inhibit tumor growth. All the data suggested P-Mg had better ability than the AO-HT-Mg. The dynamic biological system of the animal body might reduce the high pH effects for the P-Mg group, while the constantly released H₂ had a long-lasting effect on scavenging the free radicals. Because P-Mg degraded faster than AO-HT-Mg, it could release more H₂ in the body at the early stage, which made the free radical less in the animals implanted with P-Mg. So the MDA level, which is corresponding to the free radicals, was also lower in the animals implanted with P-Mg. The tumor growth rates of the animals implanted with P-Mg were also smaller at the early stage. After the metals were

implanted in the animals for 26d, AO-HT-Mg could still release large amount of H₂ because of the protection of MgO layer on the surface got by the surface modification, which made it have higher ability to inhibit the tumor growth than P-Mg.

5 Conclusion

In summary, Mg metal has the ability to inhibit tumor growth *in vivo*. The role for inhibiting tumor growth depends on the H₂ released from the biodegradation. P-Mg shows higher inhibiting ability at initial stage because it has higher H₂ releasing rate, and AO-HT-Mg shows better inhibiting ability after 26d post-operation because it could release H₂ constantly for a relative long time. It is possible to optimize its properties to inhibit tumor growth by regulating H₂ releasing rate through surface modification.

6 Acknowledgement

This work is supported by National Basic Research Program of China (973 Program, 2012CB933600), National Natural Science Foundation of China (No. 51362004, 31070848), Key Program for Science & Technology Development of China (No. 2012BAI18B04), Research Fund for the Doctoral Program of Higher Education of China (No. 20110181110064), Sichuan Province Science and Technology Innovation Team Program of China (No. 2011JTD0006) and the Jiangsu

Collaborative Innovation Center of Biomedical Functional Materials, China. The SEM observation was assisted by the Analytical and Testing Center, Sichuan University.

References

1. M. P. Staiger, A. M. Pietak, J. Huadmai and G. Dias, *Biomaterials*, 2006, **27**, 1728-1734.
2. L. Tan, X. Yu, P. Wan and K. Yang, *J Mater Sci Technol*, 2013, **29**, 503-513.
3. M. Moravej and D. Mantovani, *International journal of molecular sciences*, 2011, **12**, 4250-4270.
4. F. Witte, V. Kaese, H. Haferkamp, E. Switzer, A. Meyer-Lindenberg, C. J. Wirth and H. Windhagen, *Biomaterials*, 2005, **26**, 3557-3563.
5. H. Wang, S. Guan, Y. Wang, H. Liu, H. Wang, L. Wang, C. Ren, S. Zhu and K. Chen, *Colloids and surfaces. B, Biointerfaces*, 2011, **88**, 254-259.
6. G. Eddy Jai Poinern, S. Brundavanam and D. Fawcett, *American Journal of Biomedical Engineering*, 2013, **2**, 218-240.
7. G. Song, *Corrosion Science*, 2007, **49**, 1696-1701.
8. US Pat., 1024 1036,2004.
9. J. Li, C. Wang, J. H. Zhang, J. M. Cai, Y. P. Cao and X. J. Sun, *Brain Res*, 2010, **1328**, 152-161.
10. W. J. Zhu, M. Nakayama, T. Mori, K. Nakayama, J. Katoh, Y. Murata, T. Sato, S. Kabayama and S. Ito, *Nephrology, dialysis, transplantation : official publication of the European Dialysis and Transplant Association - European Renal Association*, 2011, **26**, 2112-2118.
11. F. R. W. Malcolm Dole, William P. Fife, *Science*, 1975, **190**, 152-154.
12. F. Wang, G. Yu, S. Y. Liu, J. B. Li, J. F. Wang, L. L. Bo, L. R. Qian, X. J. Sun and X. M. Deng, *J Surg Res*, 2011, **167**, e339-344.
13. Y. Hong, S. Chen and J. M. Zhang, *J Int Med Res*, 2010, **38**, 1893-1903.
14. I. Ohsawa, M. Ishikawa, K. Takahashi, M. Watanabe, K. Nishimaki, K. Yamagata, K. Katsura, Y. Katayama, S. Asoh and S. Ohta, *Nat Med*, 2007, **13**, 688-694.
15. M. Nan, C. Yangmei and Y. Bangcheng, *Journal of biomedical materials research. Part A*, 2014, **102**, 2644-2651.
16. G. Wu, J. M. Ibrahim and P. K. Chu, *Surface and Coatings Technology*, 2013, **233**, 2-12.
17. T. Kokubo and H. Takadama, *Biomaterials*, 2006, **27**, 2907-2915.
18. C. P. R. Mary M. Tomayko, *Cancer Chemother Pharmacol*, 1989, **24**, 148-154.
19. M. M. Jensen, J. T. Jorgensen, T. Binderup and A. Kjaer, *BMC medical imaging*, 2008, **8**, 16.
20. A. Gregory D. , Z. Ping, Jordan M. Rebecca E. M Brenton C. Katrina M. Robert J. , *American Institute of Ultrasound in Medicine*, 2010, **29**, 891-901.
21. S. P. Hussain, L. J. Hofseth and C. C. Harris, *Nature reviews. Cancer*, 2003, **3**, 276-285.
22. G. L. Makar, J. Kruger, *International Materials Reviews*, 1993, **38**, 138-153.
23. S. Keim, J. G. Brunner, B. Fabry and S. Virtanen, *Journal of biomedical materials research. Part B, Applied biomaterials*, 2011, **96**, 84-90.
24. D. Dreher, A.F. Junod, *European Journal of Cancer*, 1996, **32A**, 30-38.
25. U. N. Das, *Medical Science Monitor*, 2002, **8**, RA79-92.

26. L. Valluru, S. Dasari and R. Wudayagiri, *Oxidants and Antioxidants in Medical Science*, 2014, **3**, 15.
27. J. M. Mateo s, F. M. Sañchez-Jimeñez, *The International Journal of Biochemistry & Cell Biology*, 2000, **32**, 157-170.
28. E. M. Larry H. Rusell JR, Ramesh B. Badisa, Zhiping Zhu, Maryam Agharahimi, Ebenezer T. Oriaku, Carl B. Goodman, *Anticancer Res*, 2012, **32**, 1595-1602.
29. N. Nandakumar, T. Rengarajan, A Balamurugan, M. P Balasubramanian, *Human and Experimental Toxicology*, 2014, **33**, 504-516.
30. Y. Saitoh, Y. Yoshimura, K. Nakano, N. Miwa, *Expermental Oncoolgy*, 2009, **31**, 156-162.
31. A. S. Andrey Y. Abramov, and Michael R. Duchon, *Neuroscience*, 2007, **27**, 1129-1138.
32. J. K. Fu, Y. C. Zhu, Y. Zhao, *Materials Chemistry B*, 2014, **2**, 3538-3548.

Fig1 The structures of P-Mg and AO-HT-Mg characterized by SEM (A, B) and XRD (C). (P-Mg: untreated Mg; AO-HT-Mg: Mg treated by anodic oxidation plus heat treatment).

Fig2 The structures of P-Mg and AO-HT-Mg immersed in SBF for 24 h characterized by SEM (A, B) and XRD (C).

Fig3 The pH changes (A) and hydrogen releasing volumes (B) of P-Mg and AO-HT-Mg as a function of immersion time in SBF.

Fig4 SEM micrographs of P-Mg and AO-HT-Mg samples immersed in Dulbecco's modified Eagle's medium (DMEM) for 24 h.

Fig5 MTT assay results of MRMT-1 cultured on P-Mg and AO-HT-Mg samples for 1, 2 and 3d.

Fig6 Fluorescence coloration results of MRMT-1 cultured on P-Mg (A), AO-HT-Mg (B) samples and control group (C) for 1 (A1,B1, C1), 2 (A2,B2, C2), and 3d (A3,B3, C3). The bar is 75 μ m.

Fig7 The average OD values of free radical concentrations in MRMT-1 cultured on P-Mg and AO-HT-Mg samples for 1, 2, and 3d.

Fig8 The growth morphology changes of tumor after the 4T1/Luc cells were subcutaneously injected in the animals for 7(A1, B1, C1, D1), 10(A2, B2, C2, D2), 20(A3, B3, C3, D3) and 30d (A4, B4, C4, D4). (A: blank group; B: control group; C: P-Mg; D: AO-HT-Mg).

Fig9 The tumor growth rates in the animals implanted with P-Mg, AO-HT-Mg and control group.

Fig10 The in vivo imaging of the tumors(A) in animals at 10d (A1,B1,C1), 20d(A2,B2,C2) and 30d(A3,B3,C3) post-operation. (Control: A1, A2, A3; P-Mg: B1, B2, B3; AO-HT-Mg: C1,C2,C3). B: Blank control; C: the quantification of the fluorescence intensity in animals.

Fig11The weight changes of tumors at 10, 20 and 30 days.

Fig12MDA levels in the four group mouse serums at 10, 20 and 30 days.

Fig13H&E staining of tumors at 10(A1, B1, C1), 20(A2, B2, C2) and 30 d (A3, B3, C3) post-operation. (A: control; B: P-Mg; C: AO-HT-Mg). Image magnification is 200 \times and 400 \times respectively. The bar is 50 μ m.

Fig14The necrosis area rates of tumors with P-Mg and AO-HT-Mg at 10, 20 and 30 d post-operation.

Table1 The volume changes of tumors in different animal groups.

Table1 The volume changes of tumors in different animal groups.

	P-Mg(V/mm ³)	AO-HT-Mg(V/mm ³)	Control(V/mm ³)
7d	90.86±23.18	65.89±14.52	78.62±25.98
10d	119.55±33.6	87.04±22.11	120.35±34.75
13d	139.14±22.45	175.94±67.75	224±62
16d	238.98±38.99	296.84±108.35	349.03±79
19d	319.73±49.47	369.61±114.13	559.48±115
23d	373.5±73	523.78±181.91	673.5±163.84
26d	606.19±135.39	563.02±178.53	712.29±81.4
30d	874.53±148.37	864.59±187.95	1072.68±154.2

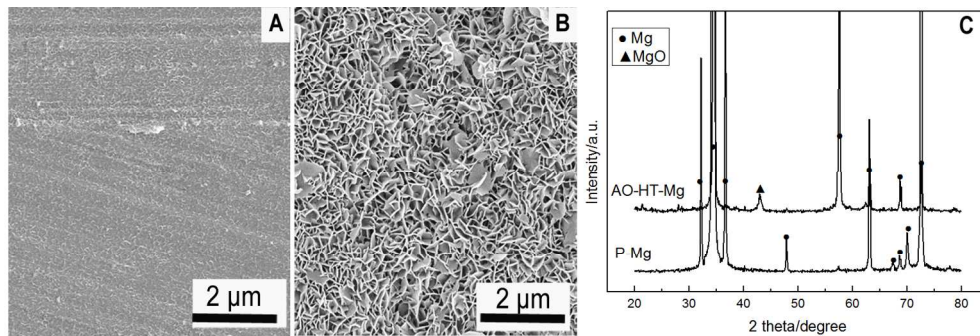


Fig 1 .The structures of P-Mg and AO-HT-Mg characterized by SEM (A, B) and XRD (C). (P-Mg: untreated Mg; AO-HT-Mg: Mg treated by anodic oxidation plus heat treatment)
143x47mm (300 x 300 DPI)

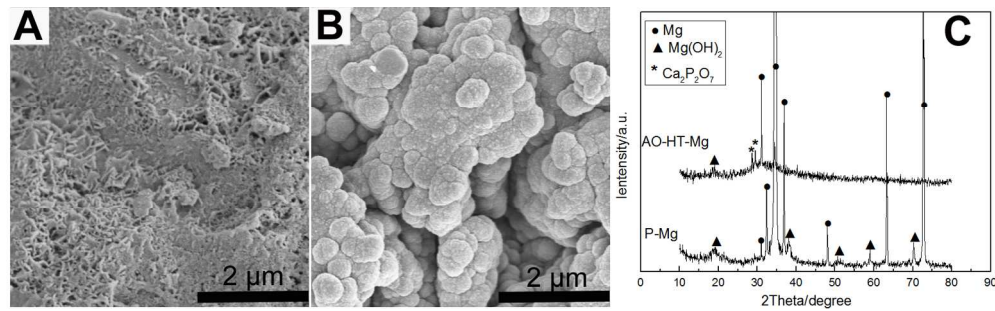


Fig 2. The structures of P-Mg and AO-HT-Mg immersed in SBF for 24 h characterized by SEM (A, B) and XRD (C)
156x46mm (300 x 300 DPI)

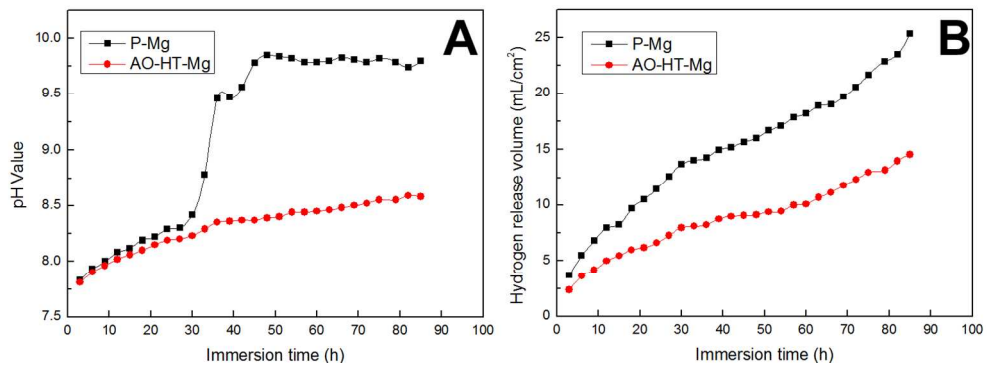


Fig 3. The pH changes (A) and hydrogen releasing volumes (B) of P-Mg and AO-HT-Mg as a function of immersion time in SBF
131x46mm (300 x 300 DPI)

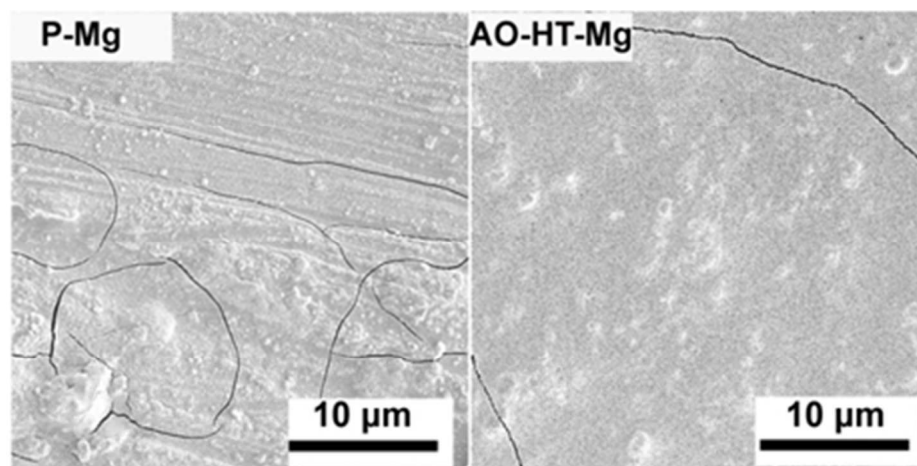


Fig4 SEM micrographs of P-Mg and AO-HT-Mg samples immersed in Dulbecco's modified Eagle's medium (DMEM) for 24 h.
78x39mm (150 x 150 DPI)

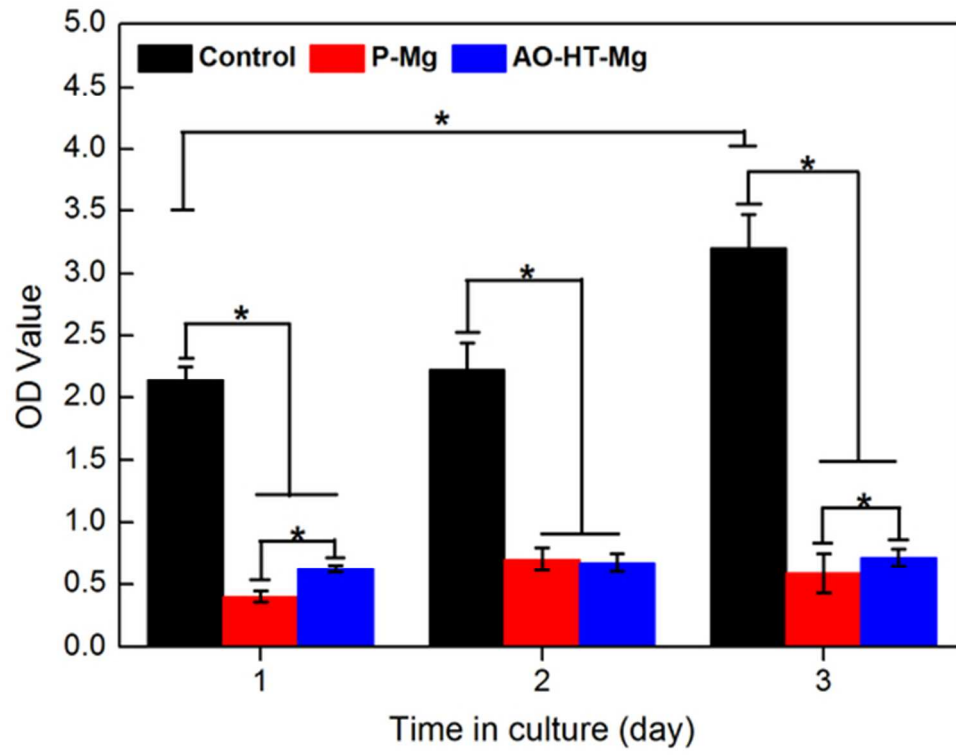


Fig5 MTT assay results of MRMT-1 cultured on P-Mg and AO-HT-Mg samples for 1, 2 and 3d.
48x36mm (300 x 300 DPI)

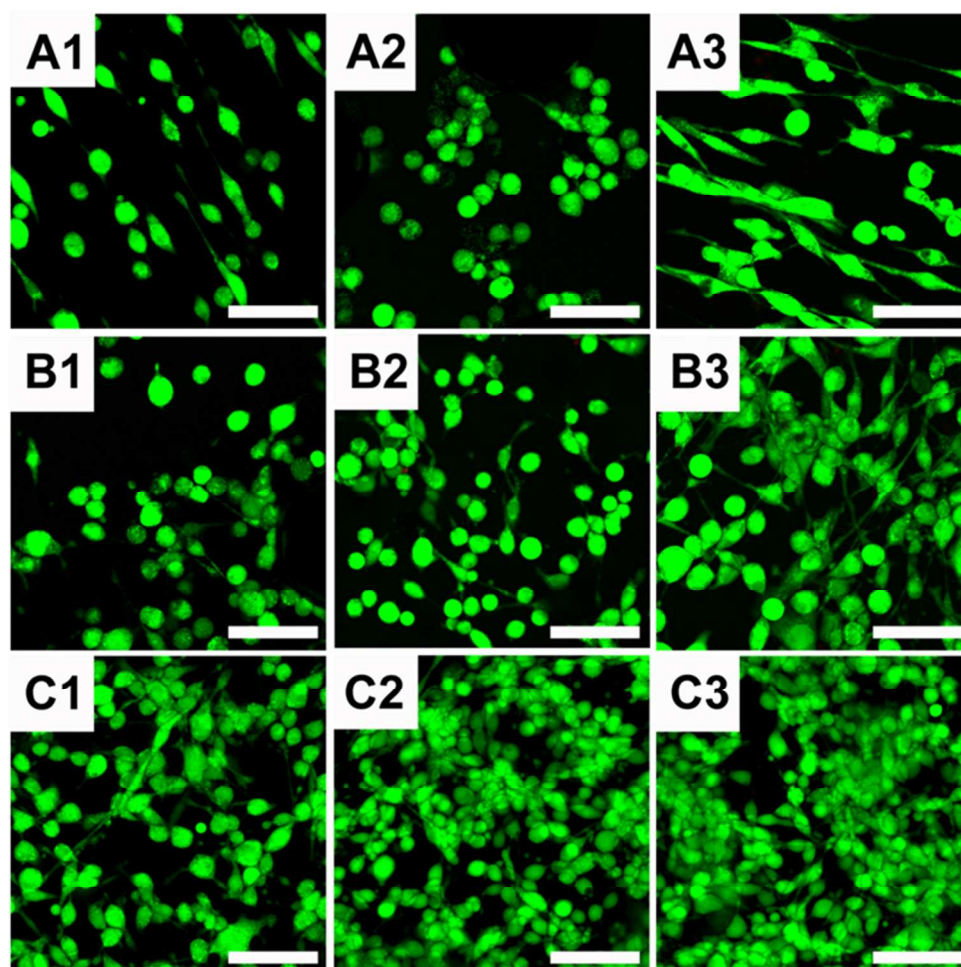


Fig6 Fluorescence coloration results of MRMT-1 cultured on P-Mg (A), AO-HT-Mg (B) samples and control group (C) for 1 (A1,B1, C1), 2 (A2,B2, C2), and 3d (A3,B3, C3). The bar is 75 μ m.
140x138mm (150 x 150 DPI)

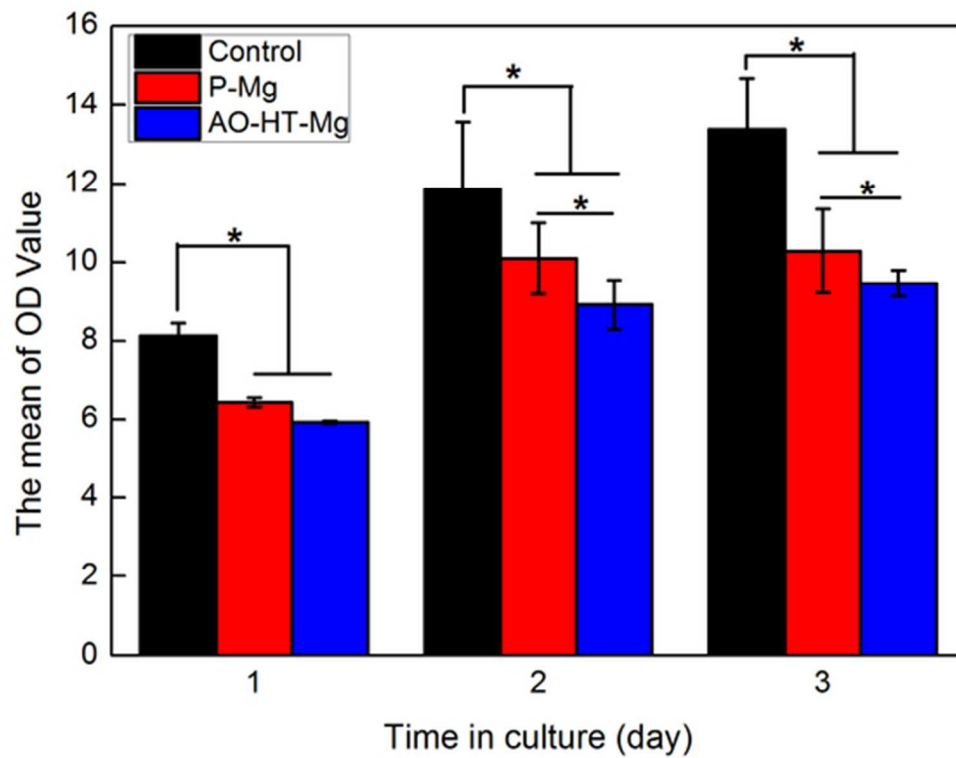


Fig7 The average OD values of free radical concentrations in MRMT-1 cultured on P-Mg and AO-HT-Mg samples for 1, 2, and 3d.
48x37mm (300 x 300 DPI)



Fig 8. The growth morphology changes of tumor after the 4T1/Luc cells were subcutaneously injected in the animals for 7(A1, B1, C1, D1), 10(A2, B2, C2, D2), 20(A3, B3, C3, D3) and 30d (A4, B4, C4, D4). (A: blank group; B: control group; C: P-Mg; D: AO-HT-Mg)
205x188mm (300 x 300 DPI)

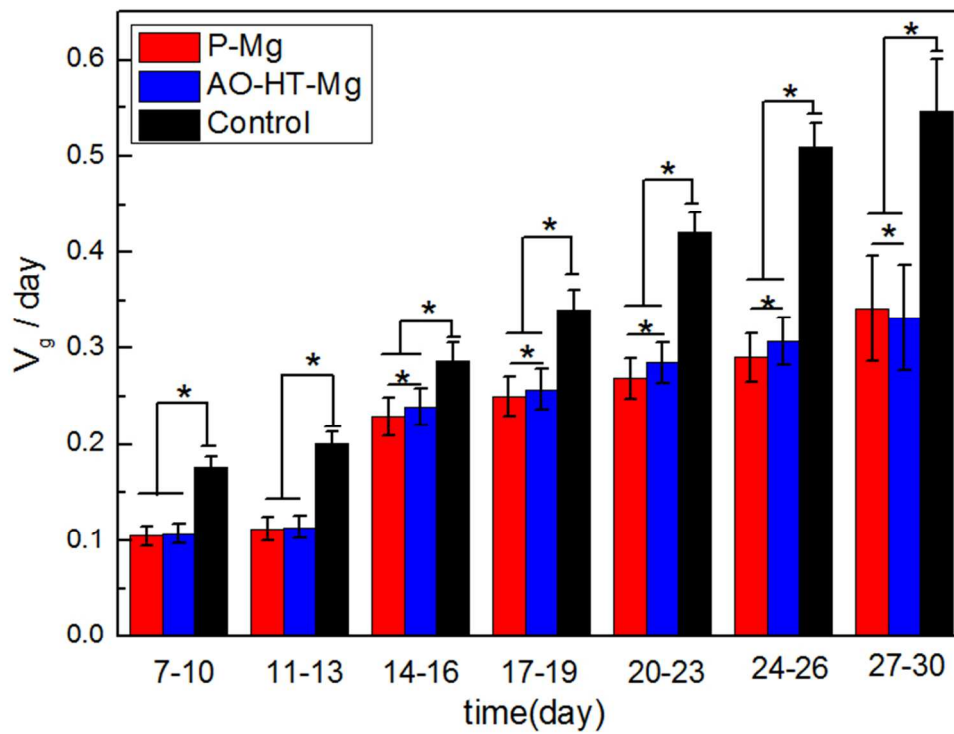


Fig9 The tumor growth rates in the animals implanted with P-Mg, AO-HT-Mg and control group.
64x48mm (300 x 300 DPI)

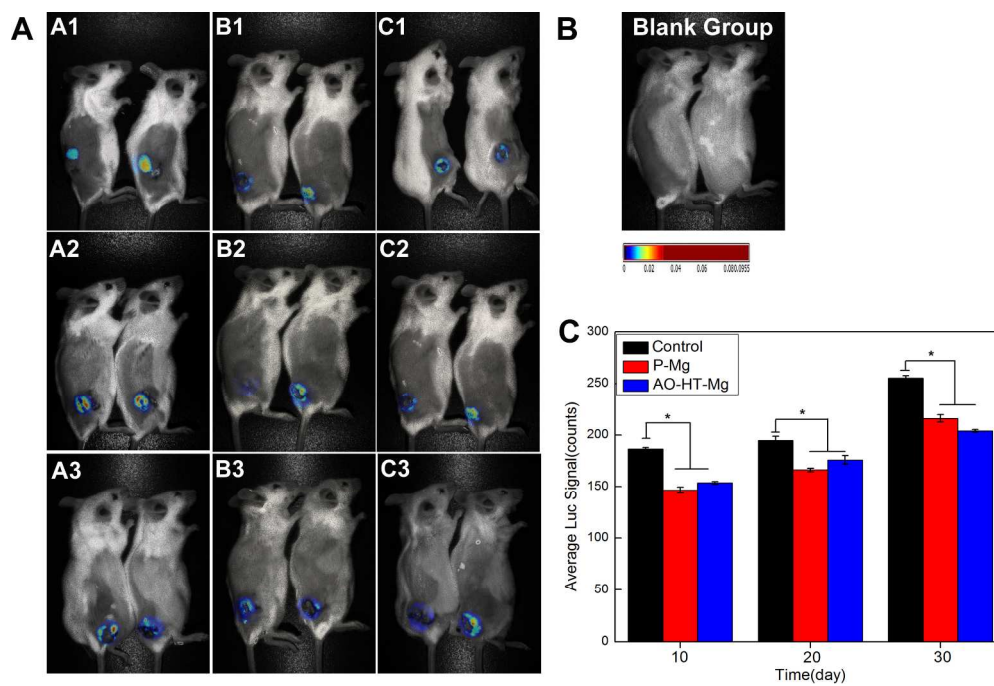


Fig10 The in vivo imaging of the tumors(A) in animals at 10d (A1,B1,C1), 20d(A2,B2,C2) and 30d(A3,B3,C3) post-operation. (Control: A1, A2, A3; P-Mg: B1, B2, B3; AO-HT-Mg: C1,C2,C3). B: blank control; C: the quantification of the fluorescence intensity in animals.
230x154mm (300 x 300 DPI)

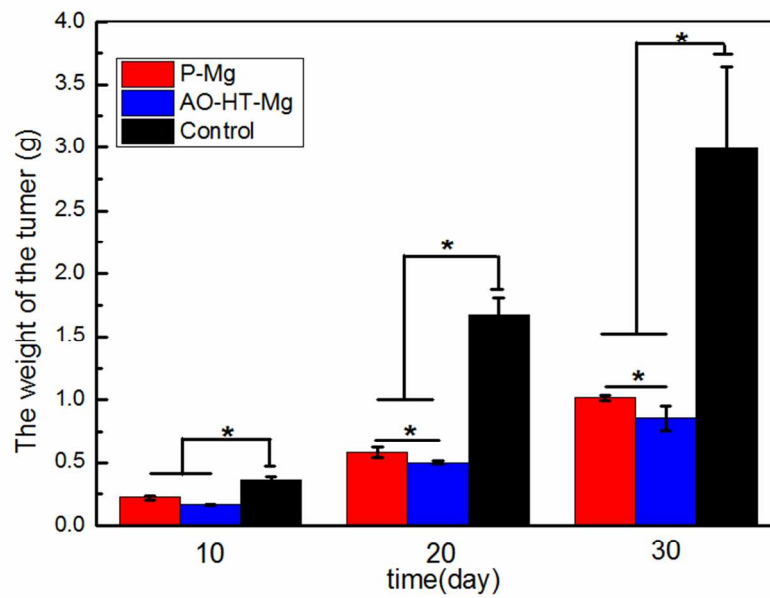


Fig 11. The weight changes of tumors at 10, 20 and 30 days
79x56mm (300 x 300 DPI)

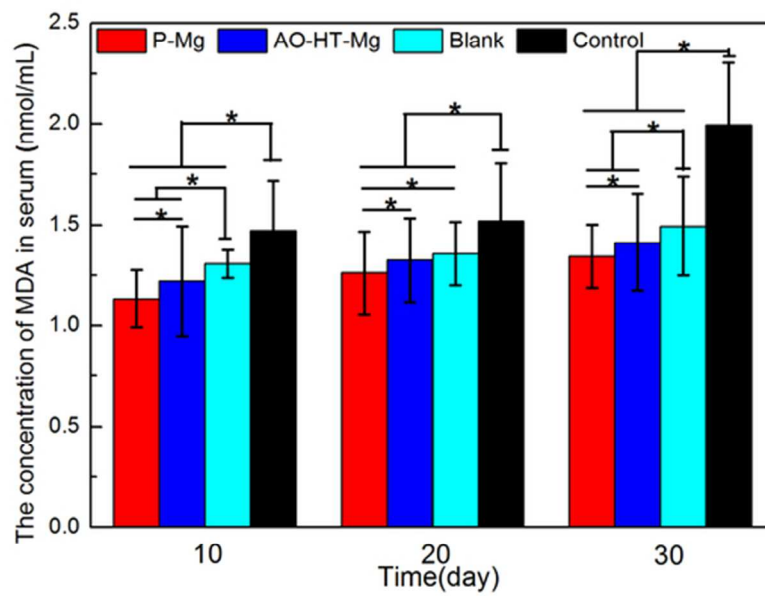


Fig 12. MDA levels in the four group mouse serums at 10, 20 and 30 days
56x39mm (300 x 300 DPI)

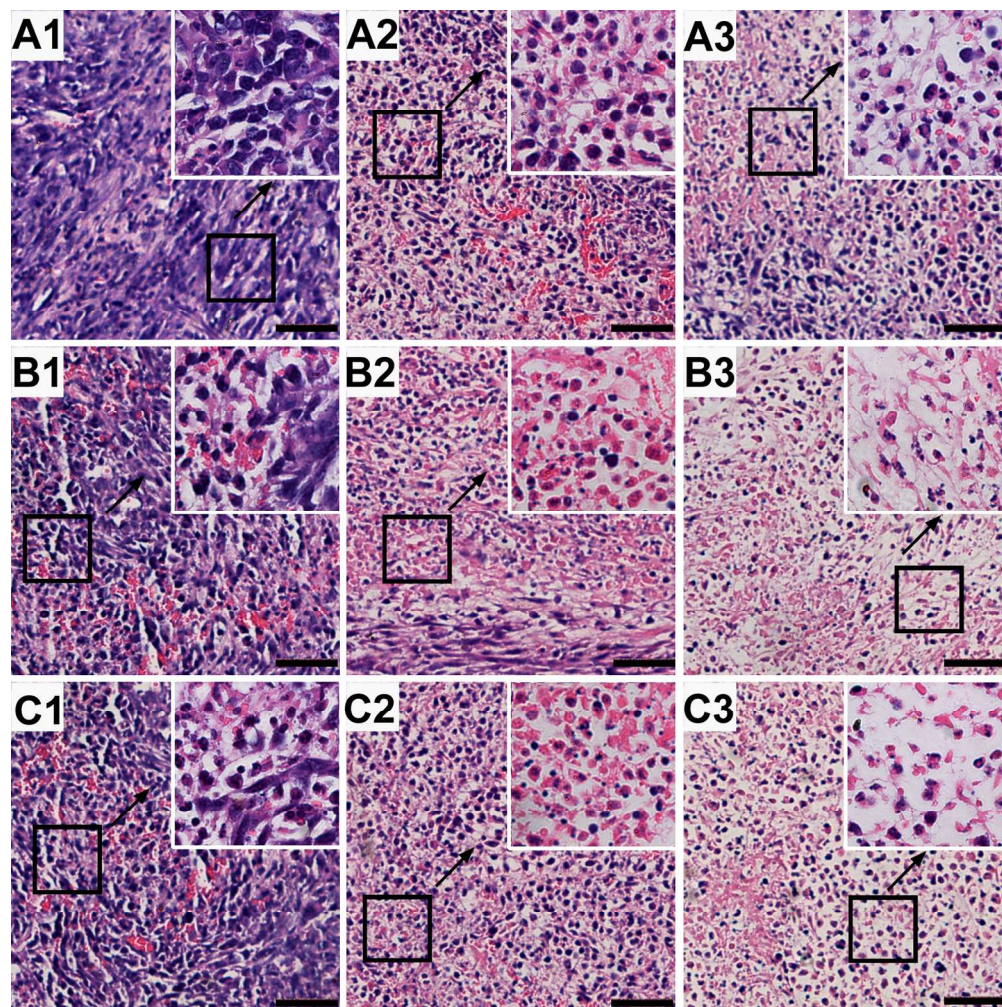


Fig 13. H&E staining of tumors at 10(A1, B1, C1), 20(A2, B2, C2) and 30 d (A3, B3, C3) post-operation. (A: control; B: P-Mg; C: AO-HT-Mg). Image magnification is 200 \times and 400 \times respectively. The bar is 50 μ m. 154x154mm (300 x 300 DPI)

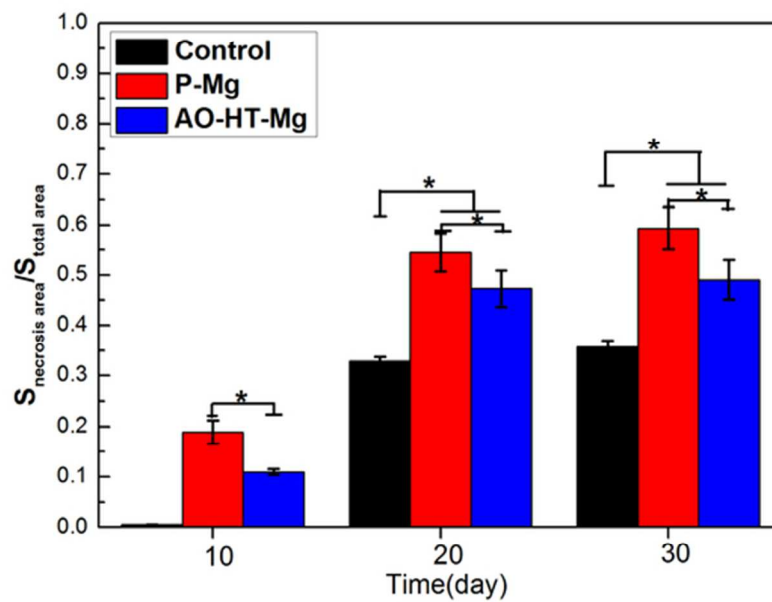


Fig14. The necrosis area rates of tumors with P-Mg and AO-HT-Mg at 10, 20 and 30 d post-operation. 56x39mm (300 x 300 DPI)

Because the free radicals in tumor cells can be removed by H_2 , the growth rate of tumor was reduced by biodegradable Mg metal with controlling the H_2 releasing rate by anodic oxidation plus heat treatment.

